International Journal of Refrigeration 105 (2019) 169–177

Contents lists available at ScienceDirect

International Journal of Refrigeration

journal homepage: www.elsevier.com/locate/ijrefrig

Oscillatory heat transfer in coated sorber beds: An analytical solution

Hesam Bahrehmand, Mehran Ahmadi, Majid Bahrami*

Laboratory for Alternative Energy Conversion (LAEC), School of Mechatronic Systems Engineering, Simon Fraser University, Surrey, BC V3T 0A3, Canada

ARTICLE INFO

Article history:
Available online 12 May 2018

Keywords:
Analytical modeling
Oscillatory heat transfer
Sorption cooling system
Thermal diffusivity
Thermal contact resistance

ABSTRACT

This paper outlines a novel closed-form analytical model that considers the thermal contact resistance (TCR) at the interface between the sorbent layer and heat exchanger (HEX). Governing energy equations with oscillatory boundary conditions are solved using an orthogonal expansion technique and closed-form relationships are reported to calculate the temperature distribution and heat flux inside the sorbent coating and HEX. In addition, a new gravimetric large pressure jump (GLAP) test bed is designed to measure the uptake of sorption material. The performance of sorber beds are evaluated in terms of specific cooling power, heat flux at HEX base and sorbent temperature standard deviation. It is found that the sorbent thermal diffusivity and TCR at the interface between the sorption coating and HEX are the key parameters that determine the thermal performance of a sorption cooling system (SCS).

Transfert de chaleur oscillatoire dans des lits à sorption enrobés: une solution analytique

Mots-clés: Modélisation analytique; Transfert de chaleur oscillatoire; Système de refroidissement à sorption; Diffusivité thermique; Résistance thermique de contact

Abbreviations

COP	Coefficient of performance
HEX	Heat exchanger
HSTR	HEX to sorbent thickness ratio
GLAP	Gravimetric large pressure jump
PVP	Polyvinylpyrrolidone
SCP	Specific cooling power, W kg^{-1}
SCS	Sorption cooling system
TCR	Thermal contact resistance, K W^{-1}
TGA	Thermogravimetric Analysis

1. Introduction

Conventional vapor compression refrigeration systems consume approximately 15% of global electrical energy and have a significant carbon footprint (Building Energy Data Book 2012). Sorption cooling systems (SCS), with working pairs such as water and silica gel or $CaCl_2$-silica gel, can be driven with low-grade heat, i.e. temperature sources below 100 °C, which is used to regenerate the sorbent material (Saha et al., 2009). However, commercialization of SCS faces fundamental challenges, including: i) low specific cooling power (SCP), due to poor heat transfer between sorber bed heat exchanger (HEX) (Wu et al., 2009; Zhao et al., 2012a; Sharafian et al., 2015) and the loose grain or coated sorbent, which ultimately leads to large sizes for SCS; and ii) low coefficient of performance (COP), which means large heat input and large condensers. Granular packed sorbent bed design offers the advantage of higher mass transfer rates, due to high void fraction between the grains, and lower cost of material and manufacturing; nonetheless, heat transfer rate in packed beds are inherently poor due to the point contacts between HEX and grains as well as to the low thermal diffusivity of the sorbent material (Freni et al., 2015). Coated sorbent beds can improve heat transfer rate, as there is a higher conductance between the heat exchanger surface and the sorbent material. However, for thin coatings (0.1–5 mm thickness), the relative thermal inertia of the HEX metal mass is considerable, which deteriorates the sorption efficiency and SCP. The importance of HEX thermal inertia results from the oscillatory heat transfer inside the sorber beds. Sorber beds need to be

* Corresponding author.
E-mail addresses: sbahrehm@sfu.ca (H. Bahrehmand), mahmadi@sfu.ca (M. Ahmadi), mbahrami@sfu.ca (M. Bahrami).

https://doi.org/10.1016/j.ijrefrig.2018.05.006
0140-7007/

Nomenclature

A	Heat transfer area, m^2
c	Specific heat capacity, J kg^{-1} K^{-1}
Fo	Fourier number
g_i	Dimensionless heat generation
h	Enthalpy, J kg^{-1}
h_{fg}	Enthalpy of evaporation, 2,498,000 J kg^{-1}
Ja	Jacob number
k	Thermal conductivity, W m^{-1} K^{-1}
p	Pressure, Pa
p_0	Saturation pressure, Pa
Q	Cooling energy, J
R_c	Dimensionless thermal contact resistance
T	Temperature, K
t	Time, s
u	Vapor velocity
X	Eigenfunction
x	Coordinate

Greek symbols

α	Thermal diffusivity, m^2 s^{-1}
β	Eigenvalue
Γ	Gamma function
η	Dimensionless coordinate
κ	Dimensionless thermal conductivity ratio
μ	Dimensionless thermal diffusivity ratio
θ	Dimensionless temperature
ρ	Density, kg m^{-3}
τ	Cycle time, s
Ω	Dimensionless angular frequency of the sorption cycles
ω	Sorbate uptake, g g^{-1} dry sorbent

Subscripts

0	Initial condition
evap	Evaporator/evaporative
sorb	Sorbent
sorp	Sorption

cooled down/heated up during sorption/desorption phases because of their exothermic/endothermic nature, and these oscillatory cool down/heat up processes are performed with the heat transfer fluid flowing through the sorber bed HEX. The oscillatory thermal behavior of SCS makes the thermal diffusivity of the sorbent coating and HEX crucially important in determining its performance. Moreover, the thermal contact resistance between the sorbent (for both coated layer and particles) and the HEX surface is key and can be up to 26% of the bulk thermal resistance inside a sorber bed (Sharafian et al., 2014), (Rezk et al., 2013). Thus, the heat transfer characteristics of sorber beds have a tremendous impact on the overall performance, SCP and COP of SCS and should be thoroughly investigated.

Mathematical modeling is a primary tool for design and optimization of sorption cooling systems that if performed properly in conjunction with experimental studies, can reduce the cost and save time. The simplest approach to study the sorber beds is thermodynamic modeling. Such models are fairly simple and cost-effective; however, they can only predict the upper performance limits of a SCS (Yong and Sumathy, 2002; Cacciola and Restuccia, 1995; Henninger et al., 2012; Anyanwu and Ogueke, 2005; Tamainot-Telto et al., 2009).

Another method to investigate the sorption beds is to adopt a lumped thermal model, which is based on the assumptions of a uniform sorbent temperature, uniform sorption of the refrigerant and thermodynamic equilibrium between the solid and gaseous phases. In such models, inter-particle mass transfer and heat transfer resistances are neglected, while the time derivative terms of temperature and sorbate uptake are considered. Energy balance, mass balance and sorption equilibrium equations are solved to acquire the temperature, pressure and sorbate uptake (Vasta et al., 2008; Khattab, 2006; Umair et al., 2014; Saha et al., (2007a), (2007b); Ahmed and Al-Dadah, 2012).

Finally, coupled heat and mass transfer models take into account the variation of sorbent temperature and sorbate uptake with time and space by including convection and diffusion terms in the governing equations. These models solve four governing equations simultaneously, i.e., mass conservation, energy balance, momentum equation, and sorption equilibrium. The complexity and nonlinearity of such coupled partial differential equations exclude the possibility of having a closed-form analytical solution. Consequently, numerical methods such as finite difference (Alam et al., 2000; Marletta et al., 2018; Ilis et al., 2018; Solmuş et al., 2018; Solmus et al., 2018; Yurtsever et al., 2018), finite volume (Mhimid, 1998; Leong and Liu, 2018; Niazmand and Dabzadeh, 2012; Zhao et al., 2012b; Mahdavikhah and Niazmand, 2013; Pan et al., 2018) and finite element methods (Anyanwu and Ogueke, 2007) are the only feasible approach, but they require high computational time.

In the present study, the temperature and uptake in sorption bed vary with time and space. The governing equations are solved using an orthogonal expansion technique, which is an analytical approach and can generate closed-form relationships (Ozisik, 1968). In addition, this model takes into consideration the TCR between sorbent and HEX while the majority of available studies have neglected it (Cacciola and Restuccia, 1995; Henninger et al., 2012; Anyanwu and Ogueke, 2005; Tamainot-Telto et al., 2009; Vasta et al., 2008; Khattab, 2006; Umair et al., 2014; Saha et al., 2007a,2007b; Ahmed and Al-Dadah, 2012; Alam et al., 2000; Marletta et al., 2018; Ilis et al., 2018; Solmuş et al., 2018a,2018b; Yurtsever et al., 2018; Mhimid, 1998; Leong and Liu, 2018; Niazmand and Dabzadeh, 2012; Zhao et al., 2012b; Mahdavikhah and Niazmand, 2013; Pan et al., 2018; Anyanwu and Ogueke, 2007). The present analytical model can accurately predict the oscillatory temperature distribution, heat transfer rate and the performance of coated sorption beds considering the TCR at the sorbent-HEX interface.

2. Governing equations

The solution domain consisting of sorbent coating and HEX is shown schematically in Fig. 1. Initially, the sorbent domain is at temperature $T_{1,0}$ and the HEX is at $T_{2,0}$. Continuity of heat flux as well as temperature jump/drop induced by TCR are considered at the interface between the sorbent coating and HEX. The following is the list of assumptions used in the development of the present model:

- The thickness of sorbent and HEX is uniform and sufficiently small compared to the other dimensions; thus, the energy equation can be assumed one-dimensional;
- The outer surface of the sorbent is assumed adiabatic. The convective heat transfer is negligible due to relatively low operating pressure (1–5 kPa) and the radiative heat transfer is negligible due to low temperature difference between the sorbent and its surrounding (10–20 K);
- Thermophysical properties of the sorbent and HEX are assumed constant;
- Convective effects of the sorbate inside the sorbent coating are negligible (Wu et al., 2009), as the coating is thin and the vapor pressure is fairly low. Therefore, Peclet number ($Pe = uL/\alpha$),

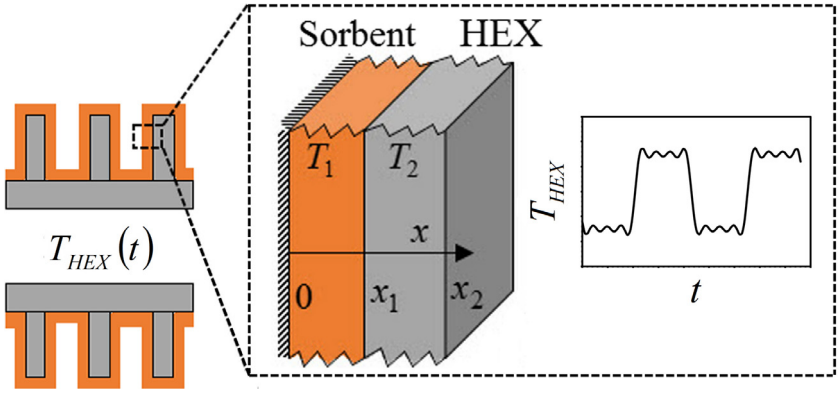

Fig. 1. Schematic diagram of the solution domain consisting of sorbent coating and HEX.

which represents the ratio of the convection term to the diffusion term in the energy equation, is small.

As such, the energy equation for the sorption layer and HEX can be written as follows.

$$\alpha_i \frac{\partial^2 T_i(x,t)}{\partial x^2} + \frac{\alpha_i}{k_i} G_i(t) = \frac{\partial T_i(x,t)}{\partial t}, \quad x_{i-1} \le x \le x_i,\ t > 0$$
$$i = 1,\ 2 \tag{1}$$

$$G_i(t) = \begin{cases} \rho_{sorb} H_{sorp} \frac{d\omega}{dt}, & i = 1 \\ 0, & i = 2 \end{cases} \tag{2}$$

where $i=1$ and $i=2$ represent the sorbent and HEX domains, respectively. The boundary conditions are

$$\frac{\partial T_1(0,t)}{\partial x} = 0 \tag{3}$$

$$k_1 \frac{\partial T_1(x_1,t)}{\partial x} = k_2 \frac{\partial T_2(x_1,t)}{\partial x} \tag{4}$$

$$-k_1 \frac{\partial T_1(x_1,t)}{\partial x} = \frac{1}{A \cdot TCR}(T_1(x_1,t) - T_2(x_1,t)) \tag{5}$$

$$T_2(x_2,t) = T_{HEX}(t) \tag{6}$$

Furthermore, the initial condition is

$$T_1(x,0) = T_{1,0},\ T_2(x,0) = T_{2,0} \tag{7}$$

Further discussion on the initial condition is provided in Section 3. The following non-dimensional variables are defined as follows.

$$\eta = \frac{x}{x_1} \qquad Fo = \frac{\alpha_2 t}{{x_1}^2} \qquad \theta = \frac{T_i(\eta, Fo) - T_{HEX}(Fo)}{T_{2,0}}$$
$$g_i = \frac{\rho H_{sorp} \alpha_i}{k_i T_0} \frac{d\omega}{dFo} \qquad \kappa_{i+1} = \frac{k_{i+1}}{k_i} \qquad R_c = \frac{k_i A \cdot TCR}{x_1}$$
$$\mu_i = \frac{\alpha_i}{\alpha_2}$$

where θ_i is the dimensionless temperature of the ith layer, the Fourier number, Fo, is the dimensionless time, η is the dimensionless coordinate, g_i is the dimensionless heat generation inside the ith layer and R_c is the dimensionless thermal contact resistance. Using the aforementioned dimensionless variables, the dimensionless energy equation as well as boundary and initial conditions can be obtained as follows.

$$\mu_i \frac{\partial^2 \theta_i(\eta, Fo)}{\partial \eta^2} + g_i(Fo) = \frac{\partial \theta_i(\eta, Fo)}{\partial Fo} + \frac{1}{T_0} \frac{dT_{HEX}(Fo)}{dFo} \tag{8}$$

$$\frac{\partial \theta_1(0, Fo)}{\partial \eta} = 0 \tag{9}$$

$$\frac{\partial \theta_1(1, Fo)}{\partial \eta} = \kappa_2 \frac{\partial \theta_2(1, Fo)}{\partial \eta} \tag{10}$$

$$-\frac{\partial \theta_1(1, Fo)}{\partial \eta} = \frac{1}{R_c}(\theta_1(1, Fo) - \theta_2(1, Fo)) \tag{11}$$

$$\theta_2(x_2/x_1, Fo) = 0 \tag{12}$$

$$\theta_1(\eta, 0) = \frac{T_{1,0} - T_{HEX}(0)}{T_{2,0}},\ \theta_2(\eta, 0) = \frac{T_{2,0} - T_{HEX}(0)}{T_{2,0}} \tag{13}$$

where $T_{HEX}(Fo)$ is the temperature at the outer surface of HEX, in which an arbitrary oscillatory profile can be applied. Fourier series in the form of Eq. (14) are used to represent this oscillatory variation of HEX temperature.

$$T_{HEX}(Fo) = a'_0 + \sum_{j=1}^{4} \left(a'_j \cos(j\Omega Fo) + b'_j \sin(j\Omega Fo) \right) \tag{14}$$

$$\Omega = \frac{2\pi}{Fo_{cycle}}$$

where Ω is the dimensionless angular frequency of the sorption cycles and a'_j, b'_j are constants in the Fourier series.

3. Modeling of sorbate uptake

The present model solves the energy equation in sorber beds, assuming 1-D heat and mass transfer. Thus, the water uptake (source term in the energy equation) should be modeled in terms of operating conditions of the sorption cycles, i.e., temperature and pressure. The isotherm of the sorbent material, obtained using an IGA-002 thermogravimetric sorption analyzer (TGA) (Hiden Isochema), is shown in Fig. 2. Sorbent material, consisting of 35 wt% $CaCl_2$, 35 wt% silica gel B150, 10 wt% PVP-40, and 20 wt% graphite flakes, was placed on the sample cell, which is held by a microbalance to measure the mass changes of the sorbent, while the temperature and pressure are controlled. The mass changes of the sorbent are collected in the range of 0.04–2.84 kPa with the pressure step of 0.2 kPa at 25 °C. More details regarding the TGA measurements can be found elsewhere (Fayazmanesh et al., 2017). Using curve fitting, a compact relationship is acquired to calculate the uptake as a function of pressure and temperature. Interestingly enough, the relationship between the uptake and temperature can be approximated with a linear function for small temperature jump (< 15 °C) as shown by the following equation:

$$\omega = m\frac{p}{p_0} + b = m\frac{p}{0.1\exp(20 - 5098/T)} + b \approx m'(p)\,T + b'(p) \tag{15}$$

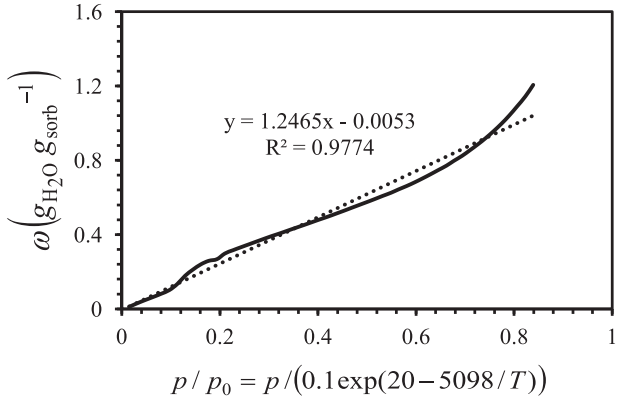

Fig. 2. TGA isotherm data for the sorbent material used.

where m and b are obtained by fitting a line to the TGA data (Fig. 2). Also, m' and b' are functions of the operating pressure at sorber bed, which will be further discussed in this section.

A new gravimetric large pressure jump (GLAP) test bed was custom-built in our lab to verify that the linear relationship between uptake and sorbent temperature obtained from TGA is valid in a real SCS. A schematic diagram of the GLAP test bed is shown in Fig. 3(a). Sorbent material was coated on 0.9 mm thick graphite sheets and installed in the GLAP test bed, see Fig. 3(b). To simulate the operation of a sorption chiller the pressure was stepped from 0.65 kPa to 2.33 kPa while the sample temperature was maintained at 40 °C. The sorber bed was placed on a precision balance (ML4002E, Mettler Toledo) with an accuracy of 0.01 g to measure the mass of the sorbate uptake. K-type thermocouples with an accuracy of 1.1 °C were passed via a feed-through in the vacuum chamber to measure the sorbent temperature. The pressure of the sorber bed and the evaporator/condenser is measured using 722B Baratron pressure transducer with the accuracy of 0.5%. The instruments were interfaced with a PC through a data acquisition system (National Instruments) and software built in the LabVIEW environment.

The variation of water uptake versus sorbent temperature measured by GLAP test bed and TGA is shown in Fig. 4 (coefficients of m' and b' in Eq. (15) are shown in Fig. 4). It can be seen that the results are in a good agreement; hence, Eq. (15) can be used to model the sorbate uptake in terms of sorbent temperature and sorber bed pressure.

It was demonstrated that variation of sorbate uptake with sorbent temperature can be approximated with a line for any given pressure of sorber bed. Since sorption cycles operate between two pressures (sorption/desorption), two constant-pressure lines can represent the sorption phases (Fig. 4). At the beginning of sorption/desorption phases, sorbent temperature increases/decreases rapidly at almost constant sorbate uptake until the bed pressure reaches the evaporator/condenser pressure (considering the pressure drop between the evaporator/condenser and the bed). Subsequently, the sorber bed is gradually cooled down/heated up to perform the sorption/desorption phases. The reason why the uptake remains almost constant during this temperature jump/drop process, is shown through a scale analysis on the energy equation in Eq. (16). Therefore, the uptake is assumed constant during this rapid process and the temperature jump/drop is taken into account as initial condition in the energy equation ($T_{1,0}$).

$$\rho c\frac{\partial T}{\partial t} = k\frac{\partial^2 T}{\partial x^2} + \rho H_{sorp}\frac{d\omega}{dt} \overset{Very\ small\ \Delta t}{\Rightarrow} \rho c\frac{\Delta T}{\Delta t} \sim \rho H_{sorp}\frac{\Delta\omega}{\Delta t}$$
$$\Rightarrow \Delta\omega \sim \frac{c\Delta T}{H_{sorp}} = \mathrm{Ja}_{sorp} < 0.005 \qquad (16)$$

4. Model development

An analytical model was developed to predict the temperature distribution and heat transfer rate inside the sorbent coating and HEX. The methodology of the solution is presented in Appendix A. Performing an integration in Eq. (A20) as well as some algebraic manipulation, the dimensionless temperature of sorbent and HEX can be obtained as follows.

$$\theta_1(\eta, Fo) = \sum_{n=1}^{\infty}\cos\left(\frac{\beta_n}{\sqrt{\mu_1}}\eta\right) \times \left[f_n^* e^{-{\beta_n}^2 Fo} + \sum_{j=1}^{4}\left\{r_{j,n}\left(\cos(j\omega Fo) - e^{-{\beta_n}^2 Fo}\right) + s_{j,n}\sin(j\omega Fo)\right\}\right] \qquad (17)$$

$$\theta_2(\eta, Fo) = \sum_{n=1}^{\infty}\left(C_{2n}\cos\left(\frac{\beta_n}{\sqrt{\mu_2}}\eta\right) + D_{2n}\sin\left(\frac{\beta_n}{\sqrt{\mu_2}}\eta\right)\right) \times \left[f_n^* e^{-{\beta_n}^2 Fo} + \sum_{j=1}^{4}\left\{r_{j,n}\left(\cos(j\omega Fo) - e^{-{\beta_n}^2 Fo}\right) + s_{j,n}\sin(j\omega Fo)\right\}\right] \qquad (18)$$

$$r_{j,n} = \frac{-j\omega {I_n}^* {\beta_n}^2}{T_0\left((j\omega)^2 + {\beta_n}^4\right)}\left(b'_j + \frac{j\omega a'_j}{{\beta_n}^2}\right)$$

$$s_{j,n} = \frac{j\omega {I_n}^* {\beta_n}^2}{T_0\left((j\omega)^2 + {\beta_n}^4\right)}\left(a'_j - \frac{j\omega b'_j}{{\beta_n}^2}\right)$$

where a'_j and b'_j are the coefficients of the Fourier series fitted to the HEX temperature profile (Eq. (14)).

5. Results and discussion

A code is developed in MATLAB to solve the transcendental equation, Eq. (A5), as well as to calculate the dimensionless temperatures of sorbent and HEX, Eqs. (17) and (18). It can be shown that the first 3 terms in the series solution ($n = 1$–3) is accurate enough to yield the temperature distributions up to seven decimal digits.

5.1. Model validation

The thermo-physical properties of sorbent and HEX are presented in Table 1. The sorbent thermo-physical properties are averaged over the range of temperature and water uptake in Fig. 4. Moreover, TCR at the silica gel/copper interface was measured by Sharafian et al. (2014) using a guarded-hot plate apparatus under vacuum pressure, and the range of 1.3–3.8 K W^{-1} was reported. As can be seen in Fig. 5, the SCP values predicted by the present model are in good agreement with those measured with GLAP test bed. It is noted that the main uncertainty in the SCP calculation is due to the mass measurement of the sorbate uptake and can result in the uncertainty of 0.5–3.5 W kg^{-1}.

5.2. Specific cooling power evaluation and parametric study

Specific cooling power (SCP) is defined as the ratio of evaporative cooling energy to the product of cycle time and dry sorbent mass, Eq. (19). For the same sorbent mass, SCP represents the rapidity of the cool down/heat up processes during sorption/desorption. To investigate various options to improve SCP, a parametric study on the oscillatory heat transfer characteristics including sorbent thermal diffusivity, HEX thermal diffusivity and thermal contact resistance, as well as the HEX to sorbent thickness ratio (HSTR) is conducted in this section. The different values

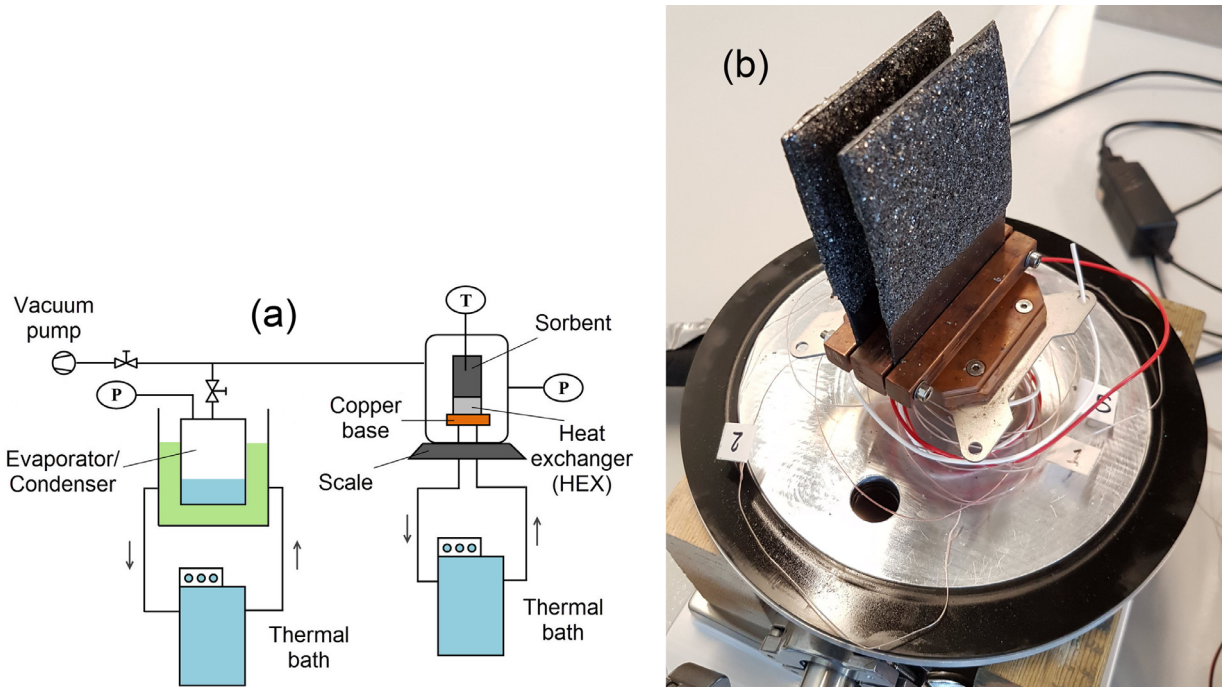

Fig. 3. (a) Schematic diagram of the GLAP test bed, (b) custom-built gravimetric large pressure jump (GLAP) test bed.

Table 1
Thermo-physical properties and geometrical characteristics of sorbent and HEX.

	k (W/mK)	ρ (kg/m^3)	c (J/kgK)	H_{sorp} (J/kg)	α (m^2/s)	Thickness (mm)
Sorbent	0.45	1213	1319	2.77e6	2.8e−7	3.4
HEX	5	1550	748	–	4.3e-6	0.9

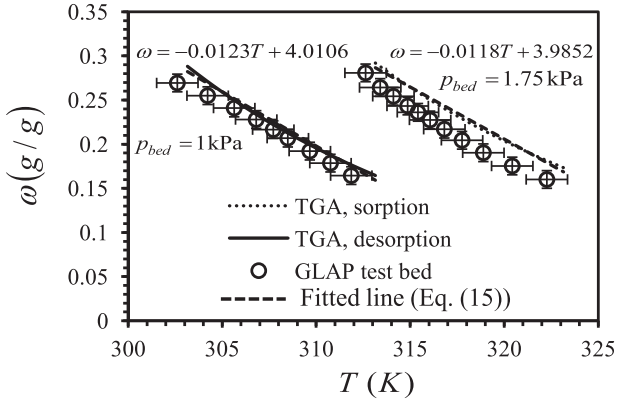

Fig. 4. Water uptake versus sorbent temperature (comparison between the results acquired from GLAP test bed and TGA).

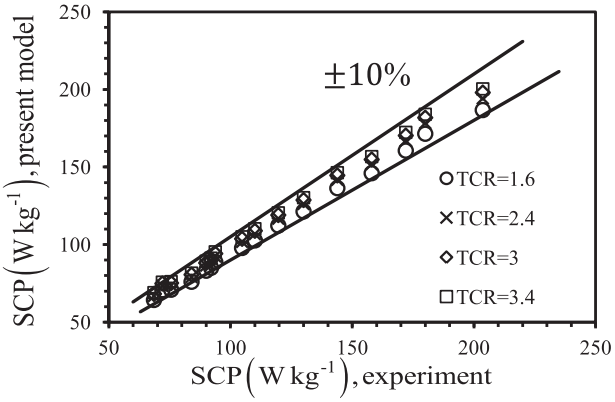

Fig. 5. Validation of the present model with the experimental data (TCR in K W^{-1}).

of oscillatory heat transfer characteristics and geometrical specifications used for parametric study are presented in Table 2.

$$SCP = \frac{Q_{evap}}{m_{sorb}\tau_{cycle}} = \frac{\Delta\omega\, h_{fg@T_{evap}}}{\tau_{cycle}} \tag{19}$$

5.2.1. Impact of thermal contact resistance (TCR)

Fig. 6 shows the impact of thermal contact resistance on dimensionless temperature inside the sorber bed, see Table 2. It can be seen that the sorbent temperature decreases/increases during sorption/desorption by decreasing TCR as the temperature drop/jump at the sorbent-HEX interface decreases. Therefore, by reducing the TCR, a sorber bed can be cooled down/heated up faster during sorption/desorption phases, consequently, the SCP of the SCS will be increased.

5.2.2. Impact of sorbent thermal diffusivity

Fig. 7 shows the impact of sorbent thermal diffusivity on the dimensionless temperature inside the sorber bed, see Table 2. It shows that the sorbent temperature decreases/increases during sorption/desorption by increasing sorbent thermal diffusivity as the heat conduction in the sorbent enhances and the sorbent thermal inertia reduces. Hence, by increasing the sorbent thermal diffusivity, the cool down/heat up processes of sorber bed are

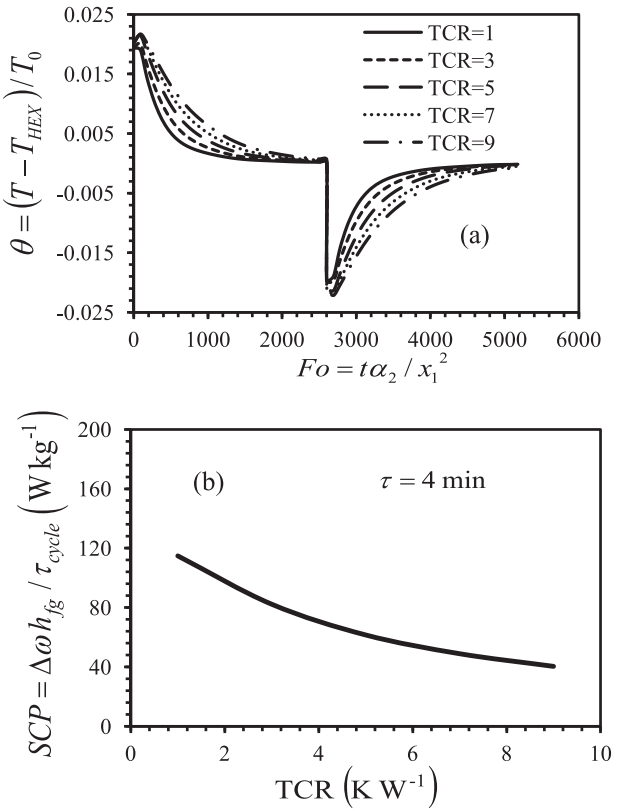

Fig. 6. Effect of thermal contact resistance on (a) dimensionless temperature at $\eta = 0$, and (b) SCP (TCR in K W^{-1}).

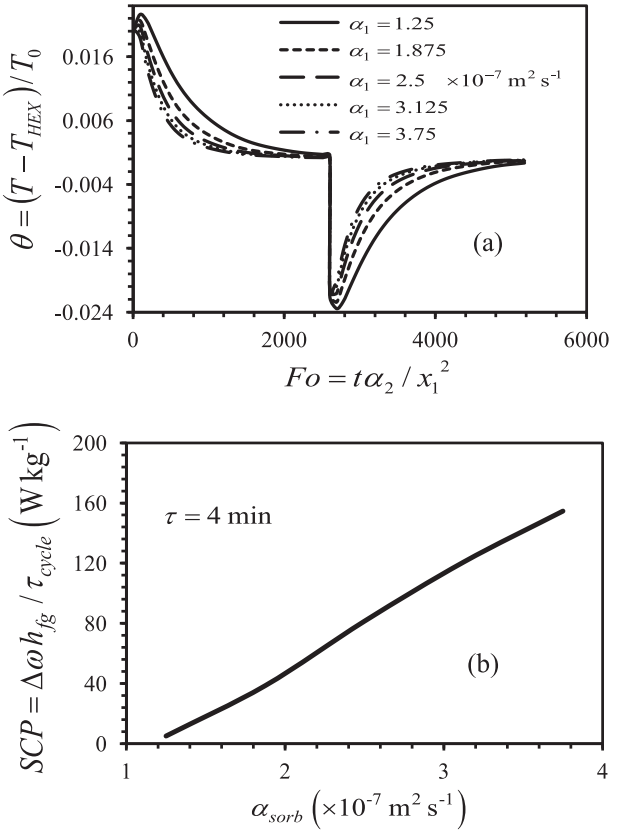

Fig. 7. Effect of sorbent thermal diffusivity on (a) dimensionless temperature at $\eta = 0$, and (b) SCP.

Table 2
Various oscillatory heat transfer characteristics and geometrical specifications used for parametric study.

Section	α_{sorb} (m^2/s)	TCR (K/W)	α_{HEX} (m^2/s)	HSTR
5.3.1	2.5e−7	1	4e−6	0.25
	2.5e−7	3	4e−6	0.25
	2.5e−7	5	4e−6	0.25
	2.5e−7	7	4e−6	0.25
	2.5e−7	9	4e−6	0.25
5.3.2	1.25e−7	3	4e−6	0.25
	1.875e−7	3	4e−6	0.25
	2.5e−7	3	4e−6	0.25
	3.125e−7	3	4e−6	0.25
	3.75e−7	3	4e−6	0.25
5.3.3	2.5e−7	3	2e−6	0.25
	2.5e−7	3	3e−6	0.25
	2.5e−7	3	4e−6	0.25
	2.5e−7	3	5e−6	0.25
	2.5e−7	3	6e−6	0.25
5.3.4	2.5e−7	3	4e−6	0.25
	2.5e−7	3	4e−6	1
	2.5e−7	3	4e−6	1.75
	2.5e−7	3	4e−6	2.5
	2.5e−7	3	4e−6	3.25
5.3.5	2.5e−7	4	4e−6	0.25
	1.5e−6	1	4e−6	0.25
	2.75e−6	0.56	4e−6	0.25
	4e−6	038	4e−6	0.25
	5.25e−6	0.3	4e−6	0.25

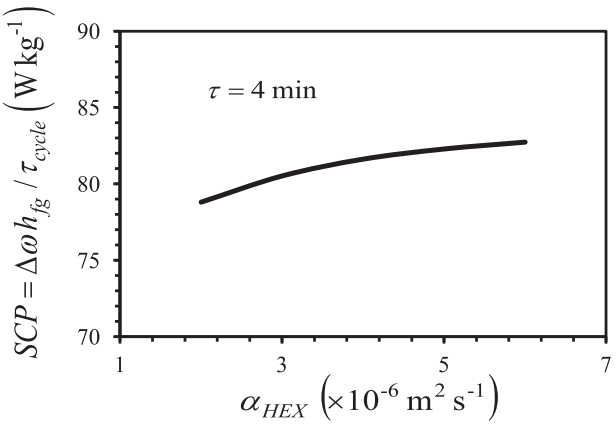

Fig. 8. Effect of HEX thermal diffusivity on SCP of SCS.

accelerated during sorption/desorption phases, thereby enhancing the SCP of the SCS.

5.2.3. Impact of HEX thermal diffusivity

Fig. 8 shows the variation of SCP with HEX thermal diffusivity, see Table 2. It is evident that the thermal diffusivity of such thin HEX has insignificant impact on SCP as the heat transfer performance is limited by the low sorbent thermal diffusivity and high TCR at sorbent/HEX interface.

5.2.4. Impact of HEX to sorbent thickness ratio (HSTR)

Fig. 9 shows the impact of HSTR on the dimensionless temperature inside the sorber bed, see Table 2. It shows that the bed temperature decreases/increases during sorption/desorption by decreasing HSTR because the relative thermal resistance of HEX to sorbent as well as the relative thermal inertia of HEX to sorbent reduce. Hence, decrease of HSTR hastens the cool down/heat up processes of sorber bed during sorption/desorption phases, which means a higher SCP of SCS.

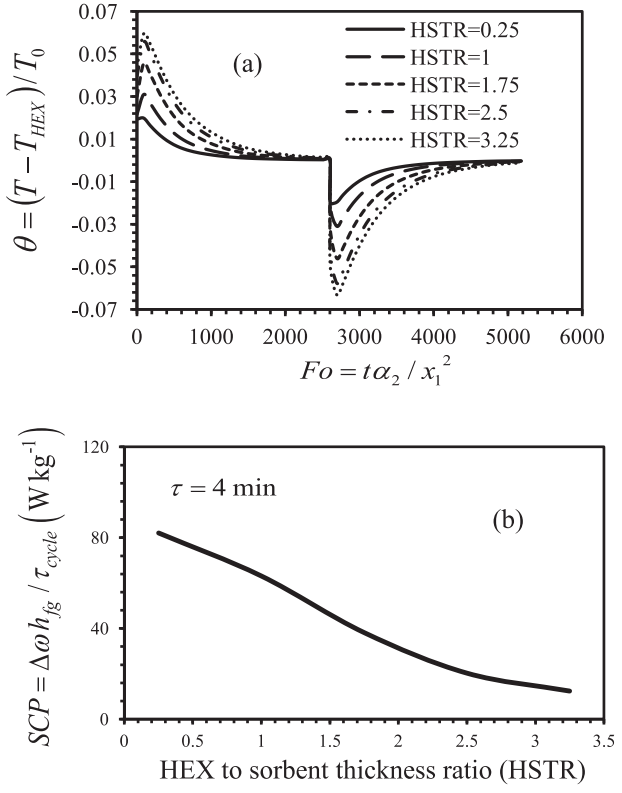

Fig. 9. Effect of HEX to sorbent thickness ratio (HSTR) on (a) dimensionless temperature at $\eta = 0$, and (b) SCP.

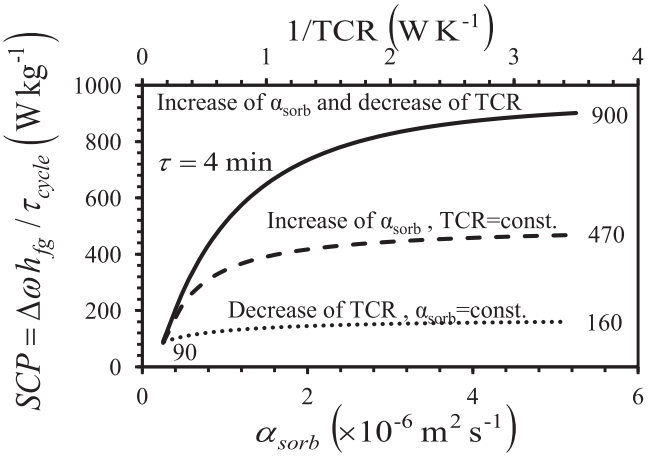

Fig. 10. Effect of sorbent thermal diffusivity and TCR on SCP.

5.2.5. Impact of sorbent thermal diffusivity and TCR

Fig. 10 shows the impact of sorbent thermal diffusivity in conjunction with TCR on the SCP of the SCS studied in this paper, see Table 2. When the sorbent–HEX TCR remains constant and α_{sorb} increases, the improvement of SCP is much higher compared to the case where α_{sorb} remains constant and TCR reduces; hence, α_{sorb} has a higher impact on the SCP compared to TCR. However, simultaneous increase of α_{sorb} and decrease of TCR results in remarkable enhancement of the SCP. For example, SCP increases from 90 to 900 W kg^{-1}, (an order of magnitude) by increasing the sorbent thermal diffusivity from 2.5e−7 to 5.25e−6 (m^2 s^{-1}) and decreasing the TCR from 4 to 0.3 (K W^{-1}). Therefore, both sorbent thermal diffusivity and TCR should be improved to enhance the SCS performance.

Table 3
Heat flux at heat exchanger base at $t = 4$ min for different oscillatory heat transfer characteristics.

α_{sorb} (m^2/s)	$\dot{q}$ (kW/m^2)	TCR (K/W)	$\dot{q}$ (kW/m^2)	α_{HEX} (m^2/s)	$\dot{q}$ (kW/m^2)
1.25e−7	0.942	1	1.320	2e−6	1.115
1.875e−7	1.033	3	1.087	3e−6	1.122
2.5e−7	1.127	5	0.961	4e−6	1.129
3.125e−7	1.201	7	0.826	5e−6	1.135
3.75e−7	1.262	9	0.720	6e−6	1.139

5.3. Evaluation of heat transfer performance

It was demonstrated that heat transfer plays a pivotal role in determining the performance of sorption cooling systems. In addition to SCP, the heat transfer performance of sorber beds can be investigated by the heat flux at the heat exchanger base (at $\eta = x_2/x_1$), which shows how much heat can be transferred from the sorbent to the heat transfer fluid through the heat exchanger. This heat flux is obtained from the following equation:

$$\dot{q}(Fo)\Big|_{\eta=\frac{x_2}{x_1}} = -k_2\frac{\partial T_2}{\partial x} = -\frac{k_2 T_{2,0}}{x_1}\frac{\partial \theta_2}{\partial \eta} = -\frac{k_2 T_{2,0}}{x_1}\sum_{n=1}^{3}\left(\frac{\beta_n}{\sqrt{\mu_2}}\right)\left(-C_{2n}\sin\left(\frac{\beta_n x_2}{\sqrt{\mu_2}x_1}\right) + D_{2n}\cos\left(\frac{\beta_n x_2}{\sqrt{\mu_2}x_1}\right)\right)\Gamma(Fo) \quad (20)$$

The effect of thermal diffusivity of the sorbent and HEX as well as TCR on the heat flux at the HEX base at $t = 4$ min are listed in Table 3. As shown, by enhancing the sorbent thermal diffusivity and reducing TCR, the base heat flux increases, whereas it increases marginally with HEX thermal diffusivity. The reason is that the sorbent and TCR are the major resistances against the heat that is transferred from the sorbent to the heat transfer fluid through HEX.

Moreover, by increasing the sorbent thermal diffusivity, the sorbent temperature profile becomes more uniform as the temperature gradient reduces. Thus, the standard deviation of the spatial variation of the sorbent temperature can represent the heat transfer performance of a sorber bed, as defined by the following equation:

$$\bar{\theta}_1(Fo) = \int_0^1 \theta_1(\eta, Fo)\, d\eta = \sum_{n=1}^{3}\frac{\sqrt{\mu_1}}{\beta_n}\sin\left(\frac{\beta_n}{\sqrt{\mu_1}}\right)\Gamma(Fo)$$

$$\sigma(Fo) = T_{2,0}\sqrt{\int_0^1 \left(\theta_1(\eta, Fo) - \bar{\theta}_1(Fo)\right)^2 d\eta} = T_{2,0}\sqrt{\sum_{n=1}^{3}\frac{\sqrt{\mu_1}}{2\beta_n}\left[\left(\cos\left(\frac{\beta_n}{\sqrt{\mu_1}}\right) - 4\bar{\theta}_1\right)\sin\left(\frac{\beta_n}{\sqrt{\mu_1}}\right) + \left(\frac{2\beta_n}{\sqrt{\mu_1}}\bar{\theta}_1^2 + \frac{\beta_n}{\sqrt{\mu_1}}\right)\right]\Gamma^2(Fo)} \quad (21)$$

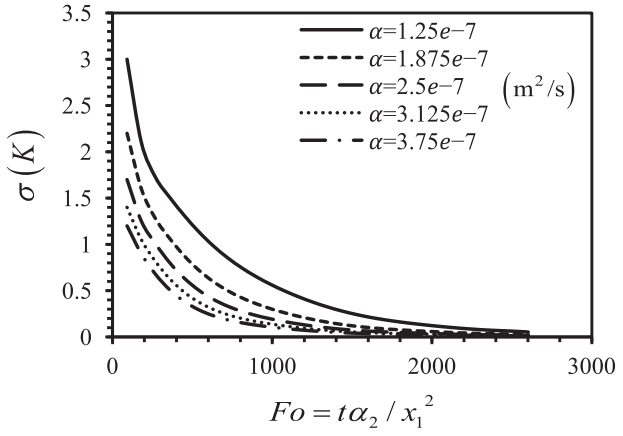

Fig. 11. Effect of sorbent thermal diffusivity on the sorbent temperature standard deviation.

Fig. 11 shows the effect of sorbent thermal diffusivity on the sorbent temperature standard deviation. It can be seen that by increasing the sorbent thermal diffusivity, the standard deviation decreases as the heat transfer inside the sorbent is improved.

6. Conclusions

A novel analytical model was developed to study the oscillatory heat transfer in sorber beds. A custom-designed gravimetric large pressure jump (GLAP) test bed was built in which large sample uptake measurements were performed and validated against TGA uptake values. A number of new graphite coated sorption beds were prepared and tested in the GLAP test bed. The present model was successfully validated with the experimental data obtained with the GLAP test bed. It was found that the sorbent thermal diffusivity, TCR at the sorbent–HEX interface and HSTR had large impacts on the performance of an SCS. Thus, by enhancing the sorbent thermal diffusivity, reducing the TCR and using thin graphite sheets, the performance and SCP of SCS can be improved remarkably.

Acknowledgment

The first author thanks the LAEC members, Dr. Khorshid Fayazmanesh, former PhD student, Dr. Claire McCague, postdoctoral fellow, and Dr. Wendell Huttema, lab engineer, for building GLAP test bed and preparing sorbent materials required to run the experiments. Furthermore, the authors gratefully acknowledge the financial support of the Natural Sciences and Engineering Research Council of Canada (NSERC) through the Automotive Partnership Canada Grant No. APCPJ 401826–10.

Appendix A

Based on Eqs. (8)–(12), the following eigen-value problem can be established (Ozisik, 1968).

$$\mu_i \frac{d^2 X_{in}(\eta)}{d\eta^2} + {\beta_n}^2 X_{in}(\eta) = 0 \tag{A1}$$

$$\frac{dX_{1n}(0)}{d\eta} = 0 \tag{A2}$$

$$\frac{dX_{1n}(1)}{d\eta} = \kappa_2 \frac{dX_{2n}(1)}{d\eta} \tag{A3}$$

$$-\frac{dX_{1n}(1)}{d\eta} = \frac{1}{R_c}(X_{1n}(1) - X_{2n}(1)) \tag{A3}$$

$$X_{2n}(x_2/x_1) = 0 \tag{A4}$$

The following transcendental equation is obtained to evaluate the eigenvalues.

$$\begin{aligned}&\frac{1}{R_c\sqrt{\mu_1}}\tan\left(\frac{\beta_n}{\sqrt{\mu_2}}\right)\tan\left(\frac{\beta_n}{\sqrt{\mu_1}}\right) - \frac{\kappa_1\beta_n}{\sqrt{\mu_1}\sqrt{\mu_2}}\tan\left(\frac{\beta_n}{\sqrt{\mu_1}}\right)\\ &+\frac{\kappa_1}{R_c\sqrt{\mu_2}} - \frac{1}{R_c\sqrt{\mu_1}}\tan\left(\frac{\beta_n x_2}{\sqrt{\mu_2}x_1}\right)\tan\left(\frac{\beta_n}{\sqrt{\mu_1}}\right)\\ &-\frac{\kappa_1\beta_n}{\sqrt{\mu_1}\sqrt{\mu_2}}\tan\left(\frac{\beta_n x_2}{\sqrt{\mu_2}x_1}\right)\tan\left(\frac{\beta_n}{\sqrt{\mu_2}}\right)\tan\left(\frac{\beta_n}{\sqrt{\mu_1}}\right)\\ &+\frac{\kappa_1}{R_c\sqrt{\mu_2}}\tan\left(\frac{\beta_n x_2}{\sqrt{\mu_2}x_1}\right)\tan\left(\frac{\beta_n}{\sqrt{\mu_2}}\right) = 0\end{aligned} \tag{A5}$$

Eigenfunctions associated with each eigenvalue are given by Eqs. (A6) and (A7).

$$X_{1n}(\eta) = \cos\left(\frac{\beta_n}{\sqrt{\mu_1}}\eta\right) \tag{A6}$$

$$X_{2n}(\eta) = C_{2n}\cos\left(\frac{\beta_n}{\sqrt{\mu_2}}\eta\right) + D_{2n}\sin\left(\frac{\beta_n}{\sqrt{\mu_2}}\eta\right) \tag{A7}$$

$$D_{2n} = \frac{\sqrt{\mu_2}\sin\left(\frac{\beta_n}{\sqrt{\mu_1}}\right)}{-\kappa_1\sqrt{\mu_1}\left(\sin\left(\frac{\beta_n}{\sqrt{\mu_2}}\right)\tan\left(\frac{\beta_n x_2}{\sqrt{\mu_2}x_1}\right) + \cos\left(\frac{\beta_n}{\sqrt{\mu_2}}\right)\right)} \tag{A8}$$

$$C_{2n} = -D_{2n}\tan\left(\frac{\beta_n x_2}{\sqrt{\mu_2}x_1}\right) \tag{A9}$$

Assuming that initial condition satisfies Dirichlet's condition, this function can be expanded over the entire range of two layers in an infinite series of eigenfunctions in the form:

$$f_i(\eta) = \sum_{n=1}^{\infty} {f_n}^* X_{in}(\eta) \tag{A10}$$

Unity can also be expanded:

$$I = \sum_{n=1}^{\infty} {I_n}^* X_{in}(\eta) \tag{A11}$$

Using the orthogonal property of eigenfunctions (Eq. (A12)), Eqs. (A13)–(A15) can be acquired.

$$\sum_{i=1}^{m}\frac{\kappa_i}{\mu_i}\int_{x_i}^{x} X_{in}(\eta)X_{in'}(\eta)d\eta = \begin{cases}0 & for\ n \neq n'\\ const. & for\ n = n'\end{cases} \tag{A12}$$

$$\begin{aligned}{f_n}^* &= \frac{1}{N}\sum_{i=1}^{m}\frac{\kappa_i}{\mu_i}\int_{x_i}^{x_{i+1}} f_i(\eta)X_{in}(\eta)d\eta\\ &= \frac{\kappa_1(T_{1,0} - T_{HEX}(0))}{N\sqrt{\mu_1}\beta_n T_{2,0}}\sin\left(\frac{\beta_n}{\sqrt{\mu_1}}\right) + \frac{\kappa_2(T_{2,0} - T_{HEX}(0))}{N\sqrt{\mu_2}\beta_n T_{2,0}}\\ &\times\left(C_{2n}\sin\left(\frac{\beta_n}{\sqrt{\mu_2}}\frac{x_2}{x_1}\right) - D_{2n}\left(\cos\left(\frac{\beta_n}{\sqrt{\mu_2}}\frac{x_2}{x_1}\right) - 1\right)\right)\end{aligned} \tag{A13}$$

$$\begin{aligned}{I_n}^* &= \frac{1}{N}\sum_{i=1}^{m}\frac{\kappa_i}{\mu_i}\int_{x_i}^{x_{i+1}} X_{in}(\eta)d\eta = \frac{1}{N}\frac{\sqrt{\mu_1}}{\beta_n}\sin\left(\frac{\beta_n}{\sqrt{\mu_1}}\right)\\ &+\frac{1}{N}\frac{\kappa_2 C_{2n}}{\sqrt{\mu_2}\beta_n}\left(\sin\left(\frac{\beta_n x_2}{\sqrt{\mu_2}x_1}\right) - \sin\left(\frac{\beta_n}{\sqrt{\mu_2}}\right)\right)\\ &-\frac{1}{N}\frac{\kappa_2 D_{2n}}{\sqrt{\mu_2}\beta_n}\left(\cos\left(\frac{\beta_n x_2}{\sqrt{\mu_2}x_1}\right) - \cos\left(\frac{\beta_n}{\sqrt{\mu_2}}\right)\right)\end{aligned} \tag{A14}$$

$$N=\sum_{i=1}^{m}\frac{\kappa_i}{\mu_i}\int_{x_i}^{x_{i+1}}{X_{in}}^2(\eta)d\eta=\frac{1}{2}\left(1+\frac{\sqrt{\mu_1}}{2\beta_n}\sin\left(\frac{2\beta_n}{\sqrt{\mu_1}}\right)\right)+\frac{\kappa_2}{\mu_2}\begin{pmatrix}\frac{1}{2}{C_{2n}}^2\left(\frac{x_2}{x_1}-1+\frac{\sqrt{\mu_2}}{2\beta_n}\left(\sin\left(\frac{2\beta_n x_2}{\sqrt{\mu_2}x_1}\right)-\sin\left(\frac{2\beta_n}{\sqrt{\mu_2}}\right)\right)\right)\\+\frac{1}{2}{D_{2n}}^2\left(\frac{x_2}{x_1}-1-\frac{\sqrt{\mu_2}}{2\beta_n}\left(\sin\left(\frac{2\beta_n x_2}{\sqrt{\mu_2}x_1}\right)-\sin\left(\frac{2\beta_n}{\sqrt{\mu_2}}\right)\right)\right)\\-\frac{\sqrt{\mu_2}}{2\beta_n}C_{2n}D_{2n}\left(\cos\left(\frac{2\beta_n x_2}{\sqrt{\mu_2}x_1}\right)-\cos\left(\frac{2\beta_n}{\sqrt{\mu_2}}\right)\right)\end{pmatrix} \tag{A15}$$

Substituting Eq. (A16) into Eq. (8) and some algebraic manipulation, Eq. (A17) can be derived.

$$\theta_i(\eta,Fo)=\sum_{n=1}^{\infty}X_{in}(\eta)\Gamma_n(Fo) \tag{A16}$$

$$\frac{d\Gamma_n(Fo)}{dFo}+{\beta_n}^2\Gamma_n(Fo)=\frac{1}{T_0}{I_n}^*\frac{dT_{HEX}(Fo)}{dFo} \tag{A17}$$

$$f_i(\eta)=\sum_{n=1}^{\infty}X_{in}(\eta)\Gamma_n(0) \tag{A18}$$

$$\Gamma_n(0)={f_n}^* \tag{A19}$$

The answer to the above ordinary differential equation is

$$\Gamma_n(Fo)=e^{-{\beta_n}^2Fo}\left({f_n}^*+\int_{Fo'=0}^{Fo'=Fo}\left[-\frac{1}{T_0}{I_n}^*\frac{dT_{HEX}(Fo')}{dFo'}\right]e^{{\beta_n}^2Fo'}dFo'\right) \tag{A20}$$

References

Ahmed, R., Al-Dadah, R., 2012. Physical and operating conditions effects on silica gel/water adsorption chiller performance. Appl. Energy 89, 142–149.

Alam, K.C.A., Saha, B.B., Kang, Y.T., Akisawa, A., Kashiwagi, T., 2000. Heat exchanger design effect on the system performance of silica gel adsorption refrigeration systems. Int. J. Heat Mass Transf. 43, 4419–4431.

Anyanwu, E., Ogueke, N., 2005. Thermodynamic design procedure for solid adsorption solar refrigerator. Renew. Energy 30, 81–96.

Anyanwu, E., Ogueke, N.V., 2007. Transient analysis and performance prediction of a solid adsorption solar refrigerator. Appl. Therm. Eng. 27, 2514–2523.

"Building Energy Data Book.," U.S. Department Energy, 2012.

Cacciola, G., Restuccia, G., 1995. Reversible adsorption heat pump: a thermodynamic model. Int. J. Refrig. 18 (2), 100–106.

Fayazmanesh, K., McCague, C., Bahrami, M., 2017. Consolidated adsorbent containing graphite flakes for heat-driven water sorption cooling systems. Appl. Therm. Eng. 123, 753–760.

Freni, A., et al., 2015. Characterization of Zeolite-Based Coatings for Adsorption Heat Pumps. Springer.

Henninger, S., Schicktanz, M., Hugenell, P., H, S., Henning, H., 2012. Evaluation of methanol adsorption on activated carbons for thermally driven chillers, part I: thermophysical characterisation. Int. J. Refrig. 35, 543–553.

Ilis, G.G., Mobedi, M., Ülkü, S., 2018. A dimensionless analysis of heat and mass transport in an adsorber with thin fins; uniform pressure approach. Int. Commun. Heat Mass Transf. 38, 790–797.

Khattab, N., 2006. Simulation and optimization of a novel solar-powered adsorption refrigeration module. Sol. Energy 80, 823–833.

Leong, K.C., Liu, Y., 2018. Numerical study of a combined heat and mass recovery adsorption cooling cycle. Int. J. Heat Mass Transf. 47 (22), 4761–4770.

Mahdavikhah, M., Niazmand, H., 2013. Effects of plate finned heat exchanger parameters on the adsorption chiller performance. Appl. Therm. Eng. 50, 939–949.

Marletta, L., Maggio, G., Freni, A., Ingrasciotta, M., Restuccia, G., 2018. A non-uniform temperature non-uniform pressure dynamic model of heat and mass transfer in compact adsorbent beds. Int. J. Heat Mass Transf. 45 (16), 3321–3330.

Mhimid, A., 1998. Theoretical study of heat and mass transfer in a zeolite bed during water desorption: validity of local thermal equilibrium assumption. Int. J. Heat Mass Transf. 41 (19), 2967–2977.

Niazmand, H., Dabzadeh, I., 2012. Numerical simulation of heat and mass transfer in adsorbent beds with annular fins. Int. J. Refrig. 35, 581–593.

Ozisik, M.N., 1968. Boundary Value Problem of Heat Conduction. International Textbook, London.

Pan, Q.W., Wang, R.Z., Wang, L.W., 2018. Comparison of different kinds of heat recoveries applied in adsorption refrigeration system. Int. J. Refrig. 55, 37–48.

Rezk, A., Al-Dadah, R.K., Mahmoud, S., Elsayed, A., 2013. Effects of contact resistance and metal additives in finned-tube adsorbent beds on the performance of silica gel/water adsorption chiller. Appl. Therm. Eng. 53 (2), 278–284.

Saha, B., El-Sharkawy, I., Chakraborty, A., Koyama, S., 2007a. Study on an activated carbon fiber-ethanol adsorption chiller: part I – system description and modelling. Int. J. Refrig. 30, 86–95.

Saha, B., El-Sharkawy, I., Chakraborty, A., Koyama, S., 2007b. Study on an activated carbon fiber-ethanol adsorption chiller: part II – performance evaluation. Int. J. Refrig. 30, 96–102.

Saha, B.B., Chakraborty, A., Koyama, S., Aristov, Y.I., 2009. A new generation cooling device employing $CaCl_2$-in-silica gel–water system. Int. J. Heat Mass Transf. 52, 516–524.

Sharafian, A., Fayazmanesh, K., Mccague, C., Bahrami, M., 2014. Thermal conductivity and contact resistance of mesoporous silica gel adsorbents bound with polyvinylpyrrolidone in contact with a metallic substrate for adsorption cooling system applications. Int. J. Heat Mass Transf. 79, 64–71.

Sharafian, A., McCague, C., Bahrami, M., 2015. Impact of fin spacing on temperature distribution in adsorption cooling system for vehicle A/C applications. Int. J. Refrig. 51, 135–143.

Solmuş, I., Rees, D.A.S., Yamal, C., Baker, D., Kaftanoğlu, B., 2018a. Numerical investigation of coupled heat and mass transfer inside the adsorbent bed of an adsorption cooling unit. Int. J. Refrig. 35, 652–662.

Solmus, I., Andrew, D., Rees, S., Yamalı, C., Baker, D., 2018b. A two-energy equation model for dynamic heat and mass transfer in an adsorbent bed using silica gel/water pair. Int. J. Heat Mass Transf. 55, 5275–5288.

Tamainot-Telto, Z., Metcalf, S.J., Critoph, R.E., Zhong, Y., Thorpe, R., 2009. Carbon – ammonia pairs for adsorption refrigeration applications : ice making, air conditioning and heat pumping. Int. J. Refrig. 32 (6), 1212–1229.

Umair, M., Akisawa, A., Ueda, Y., 2014. Performance evaluation of a solar adsorption refrigeration system with a wing type compound parabolic concentrator. Energies 7, 1448–1466.

Vasta, S., Maggio, G., Santori, G., Freni, A., Polonara, F., Restuccia, G., 2008. An adsorptive solar ice-maker dynamic simulation for north Mediterranean climate. Energy Convers. Manag. 49, 3025–3035.

Wu, W., Zhang, H., Sun, D., 2009. Mathematical simulation and experimental study of a modified zeolite 13X–water adsorption refrigeration module. Appl. Therm. Eng. 29, 645–651.

Yong, L., Sumathy, K., 2002. Review of mathematical investigation on the closed adsorption heat pump and cooling systems. Renew. Sustain. Energy Rev. 6, 305–337.

Yurtsever, A.O., Karakas, G., Uludag, Y., 2018. Modeling and computational simulation of adsorption based chemical heat pumps. Appl. Therm. Eng. 50, 401–407.

Zhao, Y., Hu, E., Blazewicz, A., 2012a. Dynamic modelling of an activated carbon–methanol adsorption refrigeration tube with considerations of interfacial convection and transient pressure process. Appl. Energy 95, 276–284.

Zhao, Y.L., Hu, E., Blazewicz, A., 2012. A non-uniform pressure and transient boundary condition based dynamic modeling of the adsorption process of an adsorption refrigeration tube. Appl. Energy 90 (1), 280–287.